J Polym Res (2013) 20:253
DOI 10.1007/s10965-013-0253-y

ORIGINAL PAPER

Characterization and antistatic behavior of SiO_2-functionalized multiwalled carbon nanotube/ poly(trimethylene terephthalate) composites

Chin-San Wu · Hsin-Tzu Liao

Received: 9 January 2013 / Accepted: 21 August 2013 / Published online: 18 September 2013
© Springer Science+Business Media Dordrecht 2013

Abstract The aim of the present work was to improve the properties of poly(trimethylene terephthalate) (PTT) by forming composites with silica (SiO_2) and multiwalled carbon nanotubes (MWCNTs). Inorganic fillers were pretreated using an in-situ sol–gel process, and then silica particles were attached to the surfaces of the multiwalled carbon nanotubes (SiO_2-MWCNTs). Maleic anhydride (MA) grafted with PTT (PTT-*g*-MA) and silica-multihydroxyl-functionalized MWCNTs (SiO_2-MWCNTs-OH) were used to improve the compatibility and dispersibility of the MWCNTs within the PTT matrix. The composites were characterized morphologically by transmission electron microscopy and chemically using Fourier transform infrared spectroscopy, ^{13}C solid-state nuclear magnetic resonance, and ultraviolet–visible spectroscopy. The PTT-*g*-MA/SiO_2-MWCNTs-OH (1 wt.%) composite exhibited significantly improved thermal properties. The functionalized PTT-*g*-MA/SiO_2-MWCNTs-OH composite also showed markedly enhanced antistatic properties. The optimal proportion of SiO_2-MWCNTs-OH in the composite was 1 wt.%; adding more than this compromised the compatibility between the organic and inorganic phases.

Keywords Poly(trimethylene terephthalate) (PTT) · Carbon nanotube · Composite · Antistatic

Introduction

Worldwide demand for high-quality aliphatic polyester plastics has soared [1, 2] because of the high strength and heat resistance of these materials [3, 4]. Manufacturers functionalize plastics to improve their properties and thereby enhance their value. Aliphatic polyester plastics such as polylactic acid (PLA), polyhydroxybutyrate (PHB), and polycaprolactone (PCL) have poor mechanical properties, limiting their use in industrial, agricultural, packaging, and fiber-forming applications. By comparison, aromatic polyester plastics such as polyethylene terephthalate (PET), polytrimethylene terephthalate (PTT), polybutylene terephthalate (PBT), and poly(butylene adipate-*co*-terephthalate) (PBAT) have good mechanical properties and processability and meet consumer requirements [5, 6]. Aromatic polyester plastics are extensively used in the textile and packaging industries [7, 8]. Biodegradable, high-performance materials have been developed using aromatic polyester PTT fiber; PTT is also one of the most popular engineering thermoplastics because of its excellent thermal and mechanical properties [9, 10].

PTT is a polymer formed by the reaction of 1,3-propanediol (1,3-PDO) with *N*,*N*′-dimethylaniline (DMA). Although many studies have focused on the crystal and chemical structures of PTT, few have explored the improved processing and mechanical performance exhibited by PTT composite materials [11, 12]. Recent studies have reported that inorganic fillers significantly enhance the heat resistance and mechanical properties of PTT. Surface-modified inorganic fillers can strengthen adhesion with the polymer matrix [13, 14]. Organic–inorganic hybrid materials are of increasing interest. Organic materials have good processability but poor mechanical properties, while inorganic materials have better high-temperature stability, durability, and electrical conductivity and enhance the mechanical strength of organic materials [15, 16]. The addition of inorganic materials to polyester plastics enhances properties such as heat resistance, mechanical properties, and antistatic behavior. However, organic materials are poor electrical conductors, and inorganic materials tend to agglomerate in organic polymers. PTT is an organic material with poor electrical conductivity that is prone to forming electrostatic complexes

C.-S. Wu (✉) · H.-T. Liao
Department of Chemical and Biochemical Engineering, Kao Yuan University, Kaohsiung County, Taiwan 82101, Republic of China
e-mail: cws1222@cc.kyu.edu.tw

with other substances. Carbon nanotubes have better conductivity than carbon black or graphite. Hence, conductive polymers made using carbon nanotubes as the filler can be effective at blocking and transmitting electromagnetic waves while retaining the original mechanical properties of the polymers [17, 18].

In this study, we attempted to improve the heat resistance, conductivity, and antistatic behavior of PTT by dispersing conductive silica-carbon nanotubes in it, thereby adding value to the composite material. PTT was blended with surface-modified silica-carbon nanotubes to form an organic–inorganic hybrid material using sol–gel technology. Firstly, dilute lactic acid was used as a catalyst to prepare the silica sol–gel and effectively disperse the modified carbon nanotubes in it in order to prepare the gel mixture of silica and carbon nanotubes. Maleic anhydride (MA) was then added for the grafting reaction; grafting enhanced the compatibility of the various composite ingredients and improved the heat resistance and antistatic behavior. In this way, the graft copolymer was formed before adding the silica-carbon nanotube inorganic materials to prepare the final composite.

Experimental

Materials

Poly(trimethylene terephthalate) (PTT) was supplied by Shell Chemical Co. (The Hague, Netherlands); tetraethoxysilane (TEOS) was obtained from Merck KGaA (Frankfurt, Germany); multiwalled carbon nanotubes (MWCNTs) (>95 % purity, 10–20 nm diameter) produced by the chemical vapor deposition method were purchased from Seasunnano Pro. Co. (Nanjing, China). Sulfuric acid (H_2SO_4, 96 %), nitric acid (HNO_3, 61 %), thionyl chloride, ethylene glycol, lactic acid, and MA were obtained from Aldrich Chemical Co. (Milwaukee, WI, USA). MA was purified before use by recrystallization from chloroform. Benzoyl peroxide (Aldrich Chemical Co.) was used as a polymerization initiator and was purified by dissolution in chloroform and reprecipitation in methanol. Other reagents were purified using conventional methods.

Grafting reaction and grafting percentage

A mixture of phenol/tetrachloroethane solution (60:40 v/v), MA, and benzoyl peroxide was added in four equal portions at 2-min intervals to molten PTT to allow grafting to take place. The reactions were performed in a nitrogen atmosphere at 40 ± 2 °C. Preliminary experiments showed that reaction equilibrium was attained in less than 12 h. Thus, reactions were allowed to progress for 12 h under stirring at 60 rpm. The product (4 g) was dissolved in 200 mL of refluxing phenol/tetrachloroethane solution (60:40 v/v) at 40 ± 2 °C, and then the solution was filtered through several layers of cheesecloth. The phenol/tetrachloroethane-soluble product in the filtrate was extracted five times using 600 mL of cold acetone per extraction. The MA loading of the phenol/tetrachloroethane-soluble polymer was determined by titration and expressed as a grafting percentage as follows: approximately 2 g of copolymer were heated for 2 h in 200 mL of refluxing phenol/tetrachloroethane solution. This solution was then titrated immediately with 0.03 N ethanolic potassium hydroxide that had been standardized against a solution of potassium hydrogen phthalate using a phenolphthalein indicator. The acid number and the grafting percentage were then calculated using the following equations [19]:

$$Acid\ \ number(mgKOH/\mathrm{g}) = \frac{V_{KOH}(mL) \times C_{KOH}(\mathrm{N}) \times 56.1}{polymer(\mathrm{g})} \quad (1)$$

$$Grafting\ \ percentage(\%) = \frac{Acid\ \ number \times 98.1}{2 \times 561} \times 100\%. \quad (2)$$

The grafting percentage was 1.08 wt.% for benzoyl peroxide and MA loadings of 0.3 and 10 wt.%, respectively.

Preparation of functionally modified SiO_2-MWCNTs-OH

The SiO_2-MWCNT and PTT modifications and the preparation of the composite material are illustrated in Scheme 1. Approximately 500 mg of crude MWCNTs were stirred in 30 mL of concentrated H_2SO_4/HNO_3 (3:1 v/v) at 50–60 °C for 50 min to oxidatively generate carboxyl functional groups (MWCNTs-COOH). During this process, the MWCNT volume expanded several-fold, suggesting that many of the bundles of MWCNTs had been dispersed into individual nanotubes. MWCNTs with pendant carbonyl chloride groups (MWCNTs-COCl) were obtained by refluxing in thionyl chloride with MWCNTs-COOH at 0–5 °C for 24 h. The conversion of the carboxylic acids into acid chlorides was accompanied by the formation of gaseous SO_2 and HCl. The SO_2 was removed continuously to lessen the extent of the reverse reaction. After the reaction was complete, unreacted $SOCl_2$ was removed using a rotary evaporator and the MWCNTs-COCl samples were dried in a vacuum oven overnight. The MWCNTs-COCl samples were highly reactive and were kept isolated from the ambient air to prevent the unintentional hydrolysis of the –COCl groups into carboxylate ions. The MWCNTs-COCl samples were allowed to react with ethylene glycol at 110–120 °C for 2 days to yield hydroxyl-functionalized MWCNTs (MWCNTs-OH). The MWCNTs-OH samples were separated by vacuum filtration through a 0.22-μm polycarbonate membrane filter (Millipore, Billerica, MA, USA) and subsequently washed with anhydrous xylenes.

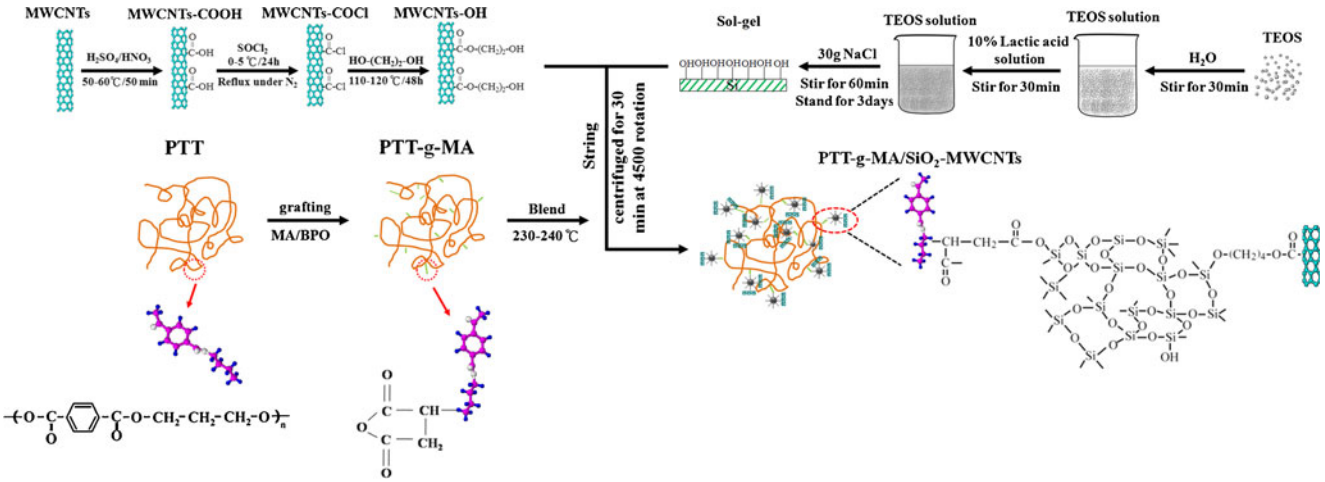

Scheme 1 Reaction scheme for the modification of PTT and SiO_2-MWCNTs-OH and the preparation of composite materials

After repeated washing and filtration steps, the solid MWCNTs-OH was dried overnight in a vacuum oven.

A mixture called "Sol A" was prepared by dissolving a stoichiometric amount of TEOS, H_2O, and lactic acid catalyst in tetrahydrofuran, stirring the solution at room temperature for 1 h, and then allowing the solution to stand for 2 days. The ratios used were as follows: lactic acid/TEOS=0.01 mol, H_2O/TEOS=2.2 mol. The MWCNTs-OH was dispersed in aqueous (deionized water) ammonia for 1 h, then the Sol A was added, and stirring continued at room temperature. After 12 h of mixing, free silica particles were removed by centrifugation (4,500 rpm). Dimethylformamide (DMF) was added to the supernatant to precipitate the product, and mixing was resumed for 30 min. The solids were removed by vacuum filtration (0.8 mm) through a nylon membrane filter. This dissolution/precipitation sequence was repeated four times. The final product (SiO_2-MWCNTs-OH), which possessed good conductive, thermal, and mechanical properties, was dried under vacuum at 70 °C for 12 h.

Preparation of the composite materials by melt-blending

Composites were prepared using a "Plastograph" 200 Nm W50EHT mixer with a blade-type rotor (C.W. Brabender Instruments, Inc., Hackensack, NJ, USA). Prior to making the composites, the SiO_2-MWCNTs-OH samples were dried in a vacuum oven at 60 °C for 2 days. Composites of PTT/SiO_2-MWCNTs-OH or PTT-*g*-MA/SiO_2-MWCNTs-OH were prepared with inorganic filler (SiO_2-MWCNTs-OH) contents of 0, 0.5, 1, and 2 wt.%. About 40 g of each composite mixture (polymer and filler) were blended at 50 rpm and 230–240 °C for 20 min with stannous octoate catalyst (0.03 wt.% catalyst loading). The PTT-*g*-MA/SiO_2-MWCNTs-OH composites were placed in a vacuum oven at 105 °C for 8 h for continued esterification. According to the ASTM D638 standard, specimens were prepared by pressing the hybrid composites into 1-mm-thick plates using a hydraulic press at 230 °C and 100 atm. After pressing, the plates were placed in a dryer for cooling. Prior to characterization, the specimens were conditioned for 24 h at a relative humidity of 50 ± 5 %.

Characterization of the hybrid composites

Fourier-transform infrared spectroscopy (FTIR; model FTS-7PC, Bio-Rad, Hercules, CA, USA) was used to investigate the grafting reaction of MA onto PTT and to verify the ester bond formation between the SiO_2-MWCNTs-OH phase and the PTT matrix. Samples subjected to FTIR analysis were ground into fine powders in a milling machine and pressed into pellets with KBr.

Solid-state ^{13}C nuclear magnetic resonance (NMR) analysis was performed using a ^{13}C NMR spectrometer (AMX 400, Bruker, Madison, WI, USA) at 100 MHz. ^{13}C NMR spectra were acquired under cross-polarization and magic-angle sample spinning; power decoupling was employed with a 90° pulse and a 4-s cycle time. Ultraviolet–visible (UV–vis) absorption spectra were recorded on a UV2001-PC spectrophotometer (Hitachi, Tokyo, Japan).

The glass transition temperature (T_g), the melting temperature (T_m), and the enthalpy of crystallization (ΔH_c) of each sample were determined using a differential scanning calorimeter (DSC 2010, TA Instruments, New Castle, DE, USA). For the DSC tests, sample sizes ranged from 4 to 6 mg, and the melting curves were obtained over a temperature range from −30 °C to 300 °C, scanned at a heating rate of 10 °C/min. A thermogravimetric analyzer (TGA 2010, TA Instruments) was used to assess whether organic–inorganic phase interactions

influenced the thermal degradation of the hybrids. Samples were placed in alumina crucibles and tested over the temperature range of 30–600 °C at a heating rate of 20 °C/min; the initial decomposition temperature (IDT) of a hybrid was taken as the shoulder in the mass loss curve.

Samples for transmission electron microscopy (TEM) analysis were dissolved in phenol/tetrachloroethane solution (60:40 v/v), which was then added dropwise onto copper grids (200 mesh copper grids, Ted Pella, Inc., Reading, CA, USA) using a micropipette. Micrographs were acquired with a transmission electron microscope (JEM-100CX II, JEOL, Tokyo, Japan) at an acceleration voltage of 100 kV.

Samples for polarized optical microscopy (POM) were examined with an Eclipse 50i POL microscope (Nikon Instruments Inc., Tokyo, Japan) equipped with a heating stage (THMS-600, Linkam Scientific Instruments Ltd., Tadworth, UK), a temperature control system (Linkam TP-92), and a video recording system. The testing specimens were prepared by sandwiching a tiny pellet of a PTT-*g*-MA/SiO_2-MWCNTs-OH composite between two glass plates. The sample was heated at 260 °C for 5 min, cooled at a rate of 2 °C/min to 210 °C, and then maintained at this temperature for 6 min to obtain the POM morphology during the crystallization process.

Electrical resistivity was measured directly on thin films (sample size: 15.0 cm × 15.0 cm × 0.1 mm) with an Ohm-Stat RT-1000 standard resistivity tester (Static Solutions Inc., Hudson, MA, USA). For the antistatic test, a circular specimen (0.1 mm in thickness and 35 mm in diameter) was rubbed with a cotton cloth for 1 min to produce static electricity, and then it was placed into a heap of tiny polystyrene balls to judge the antistatic effect. The more polystyrene balls adsorbed, the greater the static electricity produced.

Results and discussion

Structural characterization

FTIR spectroscopy was used to examine the grafting of MA onto PTT. The FTIR spectra of PTT and PTT-*g*-MA are shown in Fig. 1a and b. All of the characteristic peaks of PTT at 3,200–3,700, 1,700–1,750, and 500–1,600 cm^{-1} appeared in both polymers [20]. Two extra shoulders characteristic of carboxylic acid anhydride groups were observed at 1,786 and 1,852 cm^{-1} in the modified PTT-*g*-MA spectrum. Similar results have been reported previously [21, 22]. The shoulders represent free acid in the modified polymer PTT-*g*-MA and thus indicate the successful grafting of MA onto PTT. Figure 1c shows that the characteristic FTIR peaks of PTT and SiO_2-MWCNTs-OH were practically unchanged in the PTT/SiO_2-MWCNTs-OH hybrid, indicating only physical dispersion of the nanotubes in the polymer matrix. These peaks

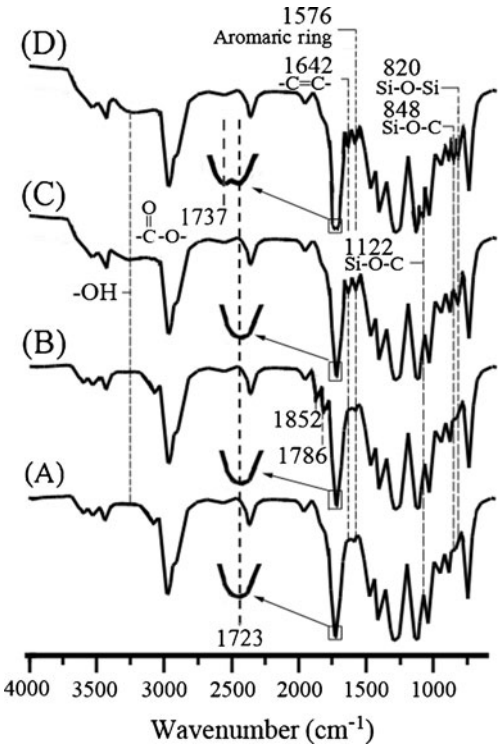

Fig. 1 FTIR spectra of (*a*) PTT, (*b*) PTT-*g*-MA, (*c*) PTT/SiO_2-MWCNTs-OH (1 wt.%), and (*d*) PTT-*g*-MA/SiO_2-MWCNTs-OH (1 wt.%)

were not observed for neat PTT and correspond to aromatic carbon atoms and SiO_2 in the SiO_2-MWCNTs-OH [−C=C−(1,575 cm^{-1} and 1,640 cm^{-1}), Si–O–Si, Si–O–C (820 cm^{-1}, 848 cm^{-1}, and 1,122 cm^{-1}), Si–OH (3,318 cm^{-1})] with no chemical interaction [23]. In contrast, the FTIR spectrum of the hybrid of PTT-*g*-MA and SiO_2-MWCNTs-OH depicted in Fig. 1d shows that the peaks at 1,786 and 1,852 cm^{-1} in Fig. 1b are shifted to 1,737 cm^{-1} as a result of condensation and ester formation between the MA groups of PTT-*g*-MA and the hydroxyl groups of SiO_2-MWCNTs-OH.

Further evidence of ester formation was provided by ^{13}C solid-state NMR spectroscopy. The ^{13}C solid-state NMR spectrum of neat PTT (Fig. 2a) was similar to that reported by Kameda et al. [24], and showed five peaks: (1) δ= 27.8 ppm, (2) δ=62.5 ppm, (3) δ=129.7 ppm, (4) δ= 133.8 ppm, and (5) δ=165.6 ppm. Compared with that of neat PTT, the ^{13}C solid-state NMR spectrum of PTT-*g*-MA (Fig. 2b) contained three additional peaks: (6) δ=35.5 ppm, (7) δ=42.1 ppm, and (8) δ=173.6 ppm. These peaks confirmed the grafting of MA onto PTT, as illustrated in Fig. 2b. The ^{13}C solid-state NMR and ^{29}Si solid-state NMR spectra of PTT/SiO_2-MWCNTs-OH, shown in Fig. 2c, also exhibited peaks that were not observed with neat PTT, which corresponded to aromatic carbon atoms and SiO_2 in the SiO_2-MWCNTs-OH: δ=120 to 125 ppm and Q_2 δ=−91 to −93 ppm, Q_3 δ=−97 to −101 ppm ,and Q_4 δ=−110 to −112 ppm [25].

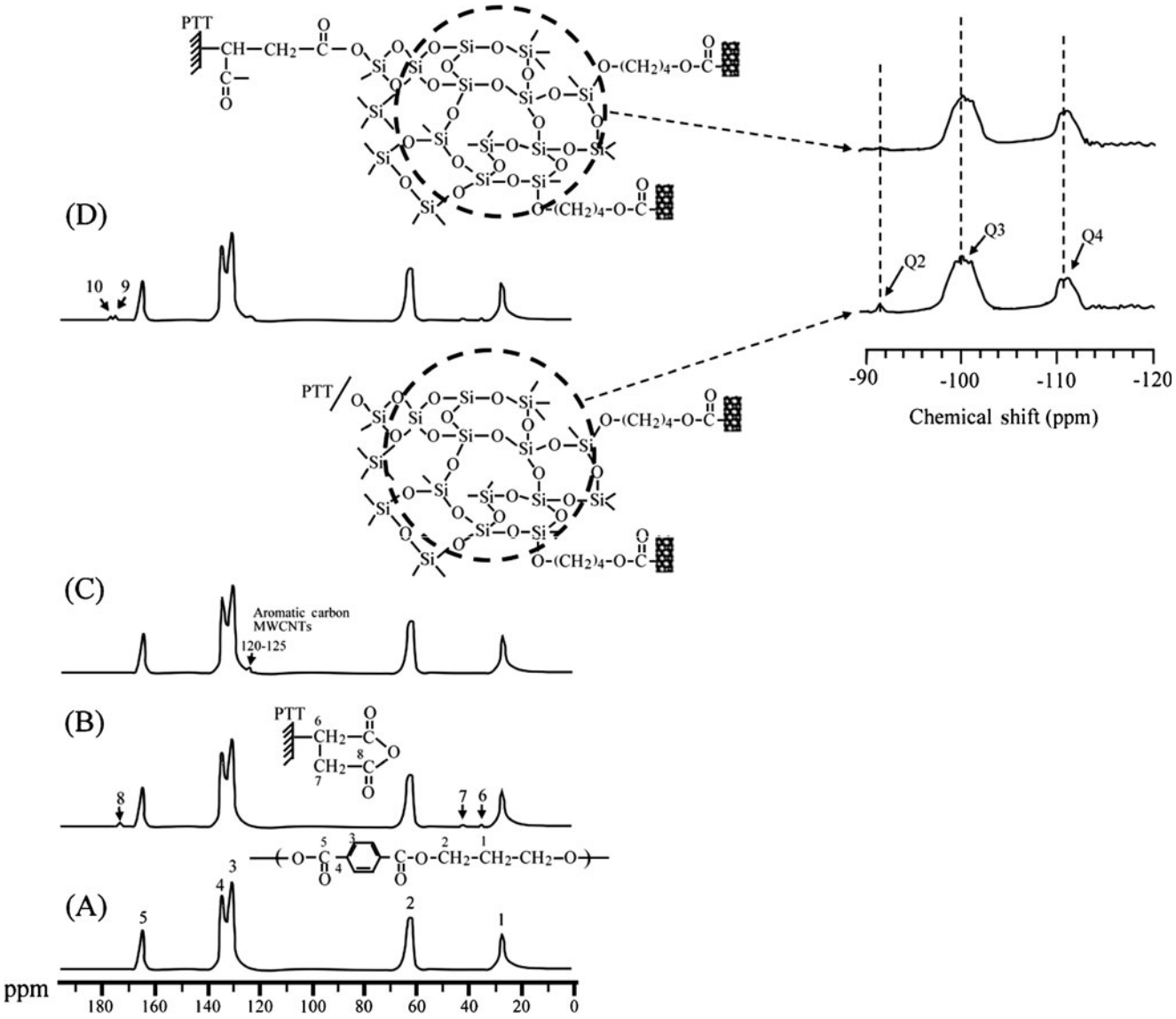

Fig. 2 ^{13}C and ^{29}Si solid-state NMR spectra of **a** PTT, **b** PTT-*g*-MA, **c** PTT-*g*-MA/SiO_2-MWCNTs-OH (1 wt.%), and **d** PTT-*g*-MA/SiO_2-MWCNTs-OH (1 wt.%)

^{13}C solid-state NMR peaks (9) and (10) (Fig. 2d), originating from the reaction between MA in PTT-*g*-MA and –OH in SiO_2-MWCNTs-OH, were found at δ=175.6 ppm and δ= 177.2 ppm; the Q2 peaks of the ^{29}Si solid-state NMR spectrum disappeared. These results, combined with the presence of FTIR peaks at 1,737 cm^{-1}, provided further evidence of ester group formation by the condensation of PTT-*g*-MA with SiO_2-MWCNTs-OH.

Dispersibility, solubility, and morphology

To further demonstrate the covalent linkage between PTT-*g*-MA and SiO_2-MWCNTs-OH, the dispersibility of the materials in mixtures of polar and partially nonpolar solvents was evaluated. The polar solvent was water and the partially nonpolar solvent was phenol/tetrachloroethane (40:60 v/v). The solvent mixture separated into upper (water) and lower (phenol/tetrachloroethane) phases. Pristine MWCNTs did not disperse in either solvent (Fig. 3a). In contrast, the relative hydrophilicity of functionalized SiO_2-MWCNTs-OH significantly enhanced the dispersibility of SiO_2-MWCNTs-OH in water (Fig. 3b) because of the association between the polar solvent and the functionally modified MWCNTs. Because the hydrophobic polymer chains of PTT-*g*-MA/SiO_2-MWCNTs-OH were soluble in phenol/tetrachloroethane, the covalently linked SiO_2-MWCNTs-OH partitioned into the lower phase (Fig. 3c). After solubilizing the PTT-*g*-MA/SiO_2-MWCNTs-OH composite in phenol/tetrachloroethane, a comparison of the degree of dispersion between the different composites was made using UV–vis absorption spectroscopy.

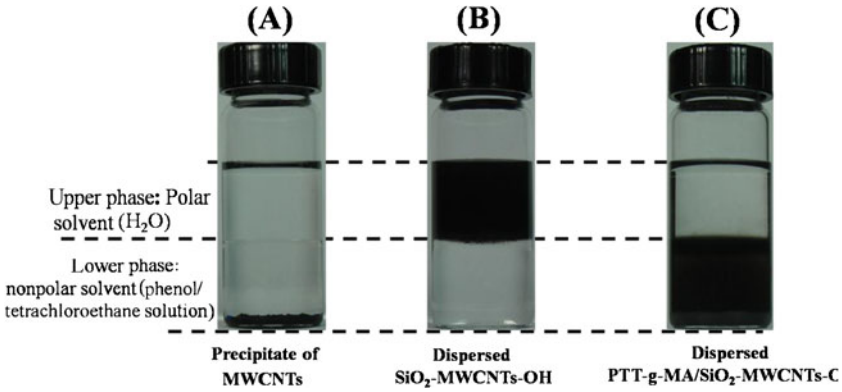

Fig. 3 Dispersion of (*a*) pure MWCNTs, (*b*) SiO_2-MWCNTs-OH, and (*c*) PTT-*g*-MA/SiO_2-MWCNTs-OH in a solution of water and (60:40, v/v) phenol/ tetrachloroethane

In situ UV–vis absorbance spectra and digital photographs are shown in Fig. 4 for phenol/tetrachloroethane solutions (40:60 v/v) of the SiO_2-MWCNTs-OH, PTT/SiO_2-MWCNTs-OH (1 wt.%), PTT-*g*-MA/SiO_2-MWCNTs-OH (1 wt.%), and PTT-*g*-MA/SiO_2-MWCNTs-OH (2 wt.%) composites. The insolubility of SiO_2-MWCNTs-OH in phenol/ tetrachloroethane is evident from line A, which shows almost no absorption from 300 to 800 nm. Both PTT/SiO_2-MWCNTs-OH and PTT-*g*-MA/SiO_2-MWCNTs-OH showed increasing solubility in the phenol/tetrachloroethane phase. For the PTT-*g*-MA/SiO_2-MWCNTs-OH hybrid, this was due to the increased binding between PTT-*g*-MA and SiO_2-MWCNTs-OH; an absorbance was observed at 360–390 nm for these composites (lines B, C and D in Fig. 4). For the PTT/SiO_2-MWCNTs-OH hybrid, there is external hydrogen bonding between PTT and SiO_2-MWCNTs-OH. Moreover, the PTT/SiO_2-MWCNTs-OH (1 wt.%) samples contained more precipitate and exhibited a lower absorbance than the samples of PTT-*g*-MA/SiO_2-MWCNTs-OH (1 wt.%). The presence of covalent links between constituents likely enhanced the dispersibility of PTT-*g*-MA/SiO_2-MWCNTs-OH (1 wt.%) compared with that of PTT/SiO_2-MWCNTs-OH (1 wt.%). Additionally, the 2 wt.% PTT-*g*-MA/SiO_2-MWCNTs-OH sample exhibited a higher degree of aggregation following hydrolysis in phenol/tetrachloroethane than the corresponding 1 wt.% sample; this result was likely due to the better dispersion in the 1 wt.% samples.

The surfaces of the PTT-*g*-MA/MWCNTs-OH and PTT-*g*-MA/SiO_2-MWCNTs-OH composites, which were soluble in phenol/tetrachloroethane solution (40:60 v/v), were imaged using TEM (Fig. 5). The latter composite had a greater diameter, which was attributed to the carbon nanotube coating on the SiO_2 particles, as reported elsewhere [26, 27]. Agglomeration was clearly evident in the PTT-*g*-MA/SiO_2-MWCNTs-OH composite containing 2 wt.% SiO_2-MWCNTs-OH. As shown in Fig. 4, the SiO_2-MWCNTs in tube A had completely precipitated at the bottom of the tube, and most of the PTT/SiO_2-MWCNTs (1 wt.%) in tube B had also precipitated; only a few particles were dispersed due to very weak associations. However, the PTT-*g*-MA/SiO_2-MWCNTs-OH (1 wt.%) in tube C was completely dispersed because of the stronger bonding between PTT-*g*-MA and SiO_2-MWCNTs-OH. Some

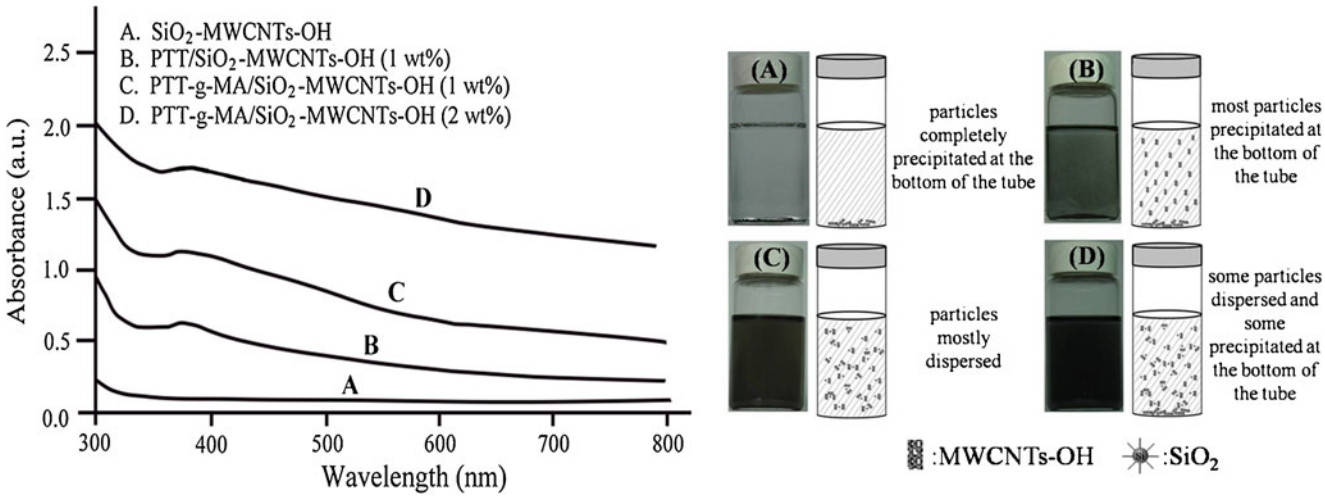

Fig. 4 Absorption spectrum of the liquid part of (*a*) SiO_2-MWCNTs-OH, (*b*) PTT/SiO_2-MWCNTs (1 wt.%), (*c*) PTT-*g*-MA/SiO_2-MWCNTs-OH (1 wt.%), and (*d*) PTT-*g*-MA/SiO_2-MWCNTs-OH (2 wt.%) dissolved in a phenol/tetrachloroethane solution (60:40, v/v) after 1 h

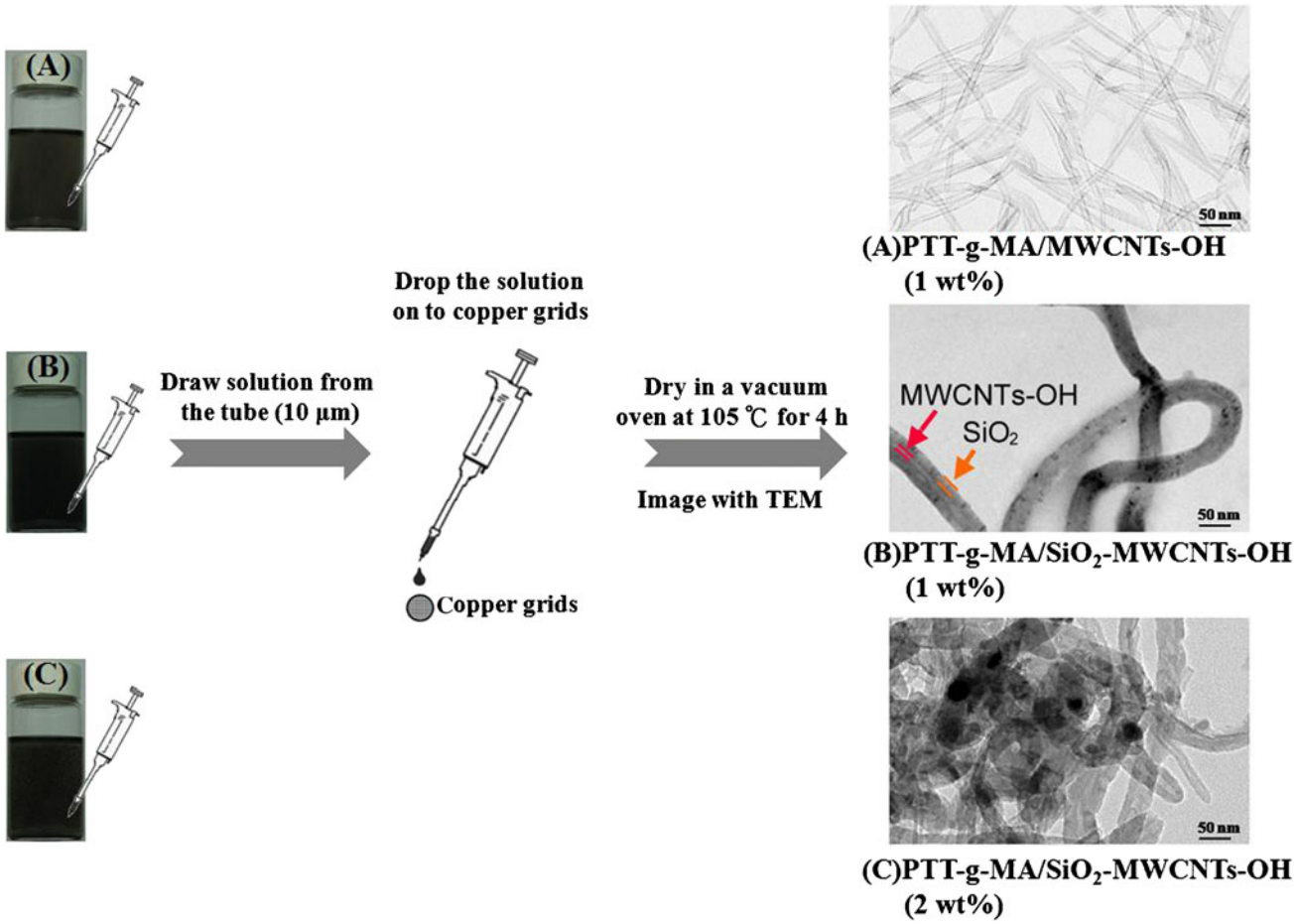

Fig. 5 Transmission electron microscopy micrographs of (*a*) PTT-*g*-MA/MWCNTs-OH (1 wt.%), (*b*) PTT-*g*-MA/SiO_2-MWCNTs-OH (1 wt.%), and (*c*) PTT-*g*-MA/SiO_2-MWCNTs-OH (2 wt.%) composites

of the PTT-*g*-MA/SiO_2-MWCNTs-OH (2 wt.%) in tube D was also dispersed, although some precipitated at the bottom of the tube because of the high SiO_2-MWCNTs-OH content. Based on the photos of tubes C and D in Fig. 4, the dispersion was optimal when the SiO_2-MWCNTs-OH content was less than 2 wt.%. Additionally, the 2 wt.% PTT-*g*-MA/SiO_2-MWCNTs-OH sample was more aggregated following hydrolysis in phenol/tetrachloroethane compared with the corresponding 1 wt.% sample. This result was likely due to the better dispersion in the 1 wt.% sample.

The electrical properties of the SiO_2-MWCNTs-OH and polymer composites relate directly to their morphologies. Generally, a good dispersion of SiO_2-MWCNTs-OH throughout the polymer matrix, effective functionalization of SiO_2-MWCNTs-OH, and strong interfacial adhesion between the two phases are required to obtain a composite material with satisfactory electrical properties.

Thermal analysis

The thermal properties (T_m, T_g, ΔH_c) of hybrids with various SiO_2-MWCNTs-OH contents were obtained from the DSC thermograms (Fig. 6a, Table 1). The glass transition temperatures (T_g) of the hybrids are associated with the cooperative motion of long-chain segments, which may be hindered by the inorganic filler (SiO_2-MWCNTs-OH). Therefore, as expected, the PTT/SiO_2-MWCNTs-OH and the PTT-*g*-MA/SiO_2-MWCNTs-OH had higher glass transition temperatures than the neat PTT and the PTT-*g*-MA copolymer. For the same filler content, Table 1 shows that the PTT-*g*-MA/SiO_2-MWCNTs-OH hybrid has a higher T_g than PTT/SiO_2-MWCNTs-OH. The greater enhancement in T_g for the PTT-*g*-MA/SiO_2-MWCNTs-OH hybrids was attributed to the formation of chemical bonds via the condensation reaction between PTT-*g*-MA and SiO_2-MWCNTs-OH; these strong bonds are able to hinder the motion of the polymer chains. For the PTT/SiO_2-MWCNTs-OH hybrids, the improvement in T_g was slight, because the SiO_2-MWCNTs-OH was only dispersed with hydrogen bonding in the PTT matrix. It was also observed that the T_g value of the PTT-*g*-MA/SiO_2-MWCNTs-OH hybrids increased with increasing SiO_2-MWCNTs-OH content to a maximum value at 1 wt.%, after which it decreased. This result may relate to the low grafting percentage (about 1.08 wt.%) of the PTT-*g*-MA copolymer;

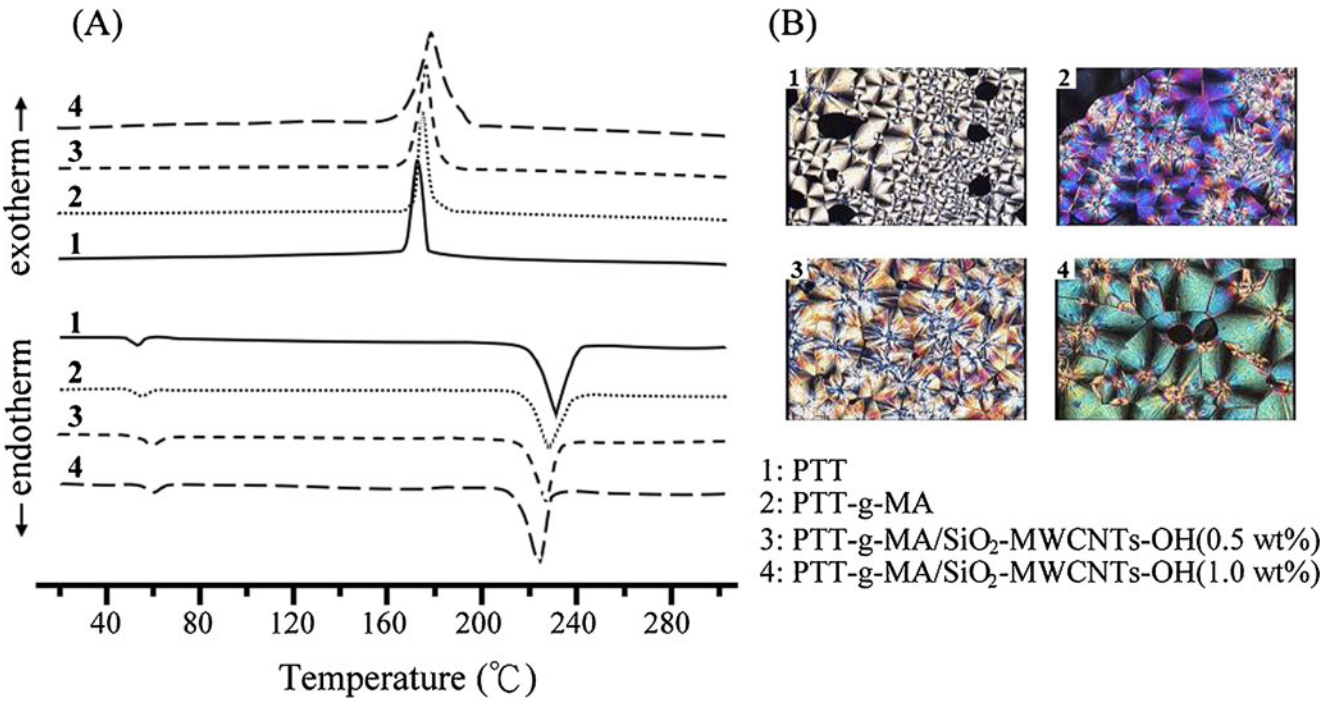

Fig. 6 DSC heating thermograms of heating curves and polarized optical microscopy morphologies of PTT-*g*-MA and its blends with different degrees of SiO_2-MWNT-OH loading at 210 °C

the increase in T_g depends on the number of functional groups in the copolymer matrix that react with the hydroxyl groups in the SiO_2-MWCNTs-OH [28]. At a SiO_2-MWCNTs-OH content of >1 wt.%, excess filler was aggregated in the polymer matrix. Such excess SiO_2-MWCNTs-OH induced the separation of the organic and inorganic phases and reduced their compatibility, causing slight increases in the T_g values.

Table 1 also shows that the addition of inorganic filler (SiO_2-MWCNTs-OH) reduced the melting temperature (T_m) for both hybrids, and that the lowest T_m occurred at the 1 wt.% filler level. Notably, for the same filler content, all of the PTT-*g*-MA/SiO_2-MWCNTs-OH hybrids had lower T_m values than their PTT/SiO_2-MWCNTs-OH equivalents. The change in thermal properties between PTT and PTT-*g*-MA composites is slight, since only a soft ester group was formed in the condensation reaction between PTT-*g*-MA and SiO2-MWCNTs-OH hybrid. A greater enthalpy of crystallization (ΔH_c) and increased nuclei spherulite size lead to higher recrystallization and larger spherulites, because SiO_2-MWCNTs-OH act as the PTT nucleating agent. Table 1 and Fig. 6 show that the ΔH_c and nuclei spherulite size increased markedly with increasing SiO_2-MWCNTs-OH content up to 1 wt.%. The observed changes for PTT-*g*-MA/SiO_2-MWCNTs-OH were likely the result of SiO_2-MWCNTs-OH inhibiting the nucleation of the polymer segments, hindering crystallization of the polymer chain, and of the SiO_2-MWCNTs-OH inhibiting crystallization of the PTT; this result was likely due to the better dispersion of the filler for the 1 wt.% samples. Additionally, the ΔH_c of PTT-*g*-MA was lower than that for neat PTT, while the ΔH_c values of the

Table 1 Thermal properties of PTT/SiO_2-MWCNTs-OH and PTT-*g*-MA/SiO_2-MWCNTs-OH hybrids

SiO_2-MWCNTs-OH (wt.%)	PTT/SiO_2-MWCNTs-OH					PTT-*g*-MA/SiO_2-MWCNTs-OH				
	T_g (°C)	T_m (°C)	ΔH_c (J/g)	IDT (°C)	Residual ash (%) (500 °C)	T_g (°C)	T_m (°C)	ΔH_c (J/g)	IDT (°C)	Residual ash (%) (500 °C)
0.0	54.3	229.2	49.9	385	0.8	53.2	227.8	48.6	375	0.8
0.5	55.7	226.4	51.3	397	19.6	57.8	225.3	53.1	406	23.6
1.0	57.2	225.7	53.6	410	27.3	60.5	224.5	56.3	422	31.8
1.5	56.4	226.0	53.3	420	35.8	58.8	224.8	55.6	431	40.9
2.0	55.6	226.3	53.1	433	43.3	57.9	225.0	55.1	445	49.2

PTT-*g*-MA/SiO_2-MWCNTs-OH blends were about 2–4 J/g higher than those of the various PTT/SiO_2-MWCNTs-OH samples. This behavior is attributable to the formation of the ester carbonyl functional group from the reaction between the –OH group of SiO_2-MWCNTs-OH and the MA group of PTT-*g*-MA.

The IDT values of the hybrids were obtained from the shoulder of the mass loss curves of PTT/SiO_2-MWCNTs-OH (not shown here) and PTT-*g*-MA/SiO_2-MWCNTs-OH (Fig. 7); the results are summarized in Table 1. Figure 8 shows that there was no weight loss up to 330 °C; above this temperature, only single-step degradation occurred for all of the polymers. For neat PTT, mostly statistical intramolecular decomposition with the formation of crotonate end groups takes place during thermal decomposition. PTT-*g*-MA had a lower IDT value than PTT, providing evidence that the onset of PTT thermal decomposition was decreased by the presence of carboxylate end groups [29]. Compared with the neat PTT or the PTT-*g*-MA copolymer, the PTT/SiO_2-MWCNTs or PTT-*g*-MA/SiO_2-MWCNTs-OH hybrids had higher IDT values and higher amounts of residual ash (Fig. 7). For the same filler content, Table 1 shows that the PTT-*g*-MA/SiO_2-MWCNTs-OH hybrid had a higher IDT value than that for PTT/SiO_2-MWCNTs-OH. This result was attributed to the difference in interfacial forces in the two hybrids, i.e., the weaker hydrogen bonds in PTT/SiO_2-MWCNTs-OH compared with the stronger coordination sites associated with the MA groups of PTT-*g*-MA and the –OH group of SiO_2-MWCNTs-OH. A comparison between PTT-*g*-MA and PTT-*g*-MA/SiO_2-MWCNTs-OH shows that the increase in IDT was about 41 °C with 1 wt.% SiO_2-MWCNTs-OH, but only about 23 °C when the SiO_2-MWCNTs-OH content was increased from 1 wt.% to 2 wt.%. This result further confirmed that the optimal loading of SiO_2-MWCNTs-OH was

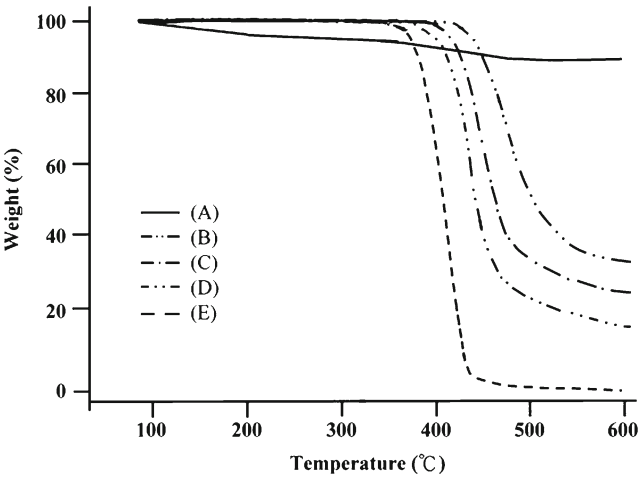

Fig. 7 TGA analysis (in N_2) of (*a*) MWCNTs-OH, (*b*) PTT-*g*-MA/SiO_2-MWCNTs-OH (2 wt.%), (*c*) PTT-*g*-MA/SiO_2-MWCNTs-OH (1 wt.%), (*d*) PTT-*g*-MA/SiO_2-MWCNTs-O (0.5 wt.%), and (*e*) PTT

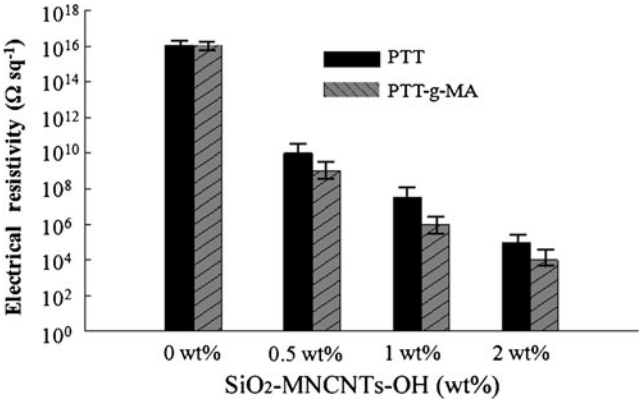

Fig. 8 Electrical resistivity of PTT/SiO_2-MWCNTs and PTT-*g*-MA/SiO_2-MWCNTs-OH composites (0, 0.5, 1, and 2 wt.%)

1 wt.%; excess SiO_2-MWCNTs-OH caused separation of the organic and inorganic phases and impaired their compatibility and dispersibility (Fig. 5c).

Additionally, the residual yields of the PTT-*g*-MA/SiO_2-MWCNTs-OH composites increased with increasing SiO_2-MWCNTs-OH content, indicating that thermal decomposition of the polymer matrix was retarded in the PTT-*g*-MA/SiO_2-MWCNTs-OH composites. This result was attributed to a physical barrier effect; the SiO_2-MWCNTs-OH prevented the transport of decomposition products in the polymer composites. Similar observations have been reported for polymer/SiO_2-MWCNTs-OH composites, the thermal stabilities of which were improved by a physical barrier effect and enhanced by ablative reassembling of MWCNT layers [30]. Thus, the TGA results demonstrated that the incorporation of a small quantity of SiO_2-MWCNTs-OH significantly improved the thermal stability of the PTT-*g*-MA/SiO_2-MWCNTs-OH composites.

Electrical conductivity and antistatic behavior

Electrical resistivity was used as a measure of the electrical conductivity of the PTT/SiO_2-MWCNTs and PTT-*g*-MA/SiO_2-MWCNTs-OH hybrid materials (conductivity is the reciprocal of resistivity); the results are depicted in Fig. 8. A marked decrease in electrical resistivity was observed with increasing SiO_2-MWCNTs-OH content up to 1 wt.%, above which the electrical resistivity decreased slightly. The reduced electrical resistivity of PTT-*g*-MA/SiO_2-MWCNTs-OH was attributed to inhibited polymer motion, which prohibited the chain rearrangement and reorganization required for solidification. As expected, both PTT/SiO_2-MWCNTs-OH and PTT-*g*-MA/SiO_2-MWCNTs-OH had lower electrical resistivities than pure PTT and PTT-*g*-MA. The decrease in electrical resistivity was greater for PTT-*g*-MA/SiO_2-MWCNTs-OH than for PTT/SiO_2-MWCNTs-OH, presumably because of ester bond formation, as discussed previously. Ester linkages

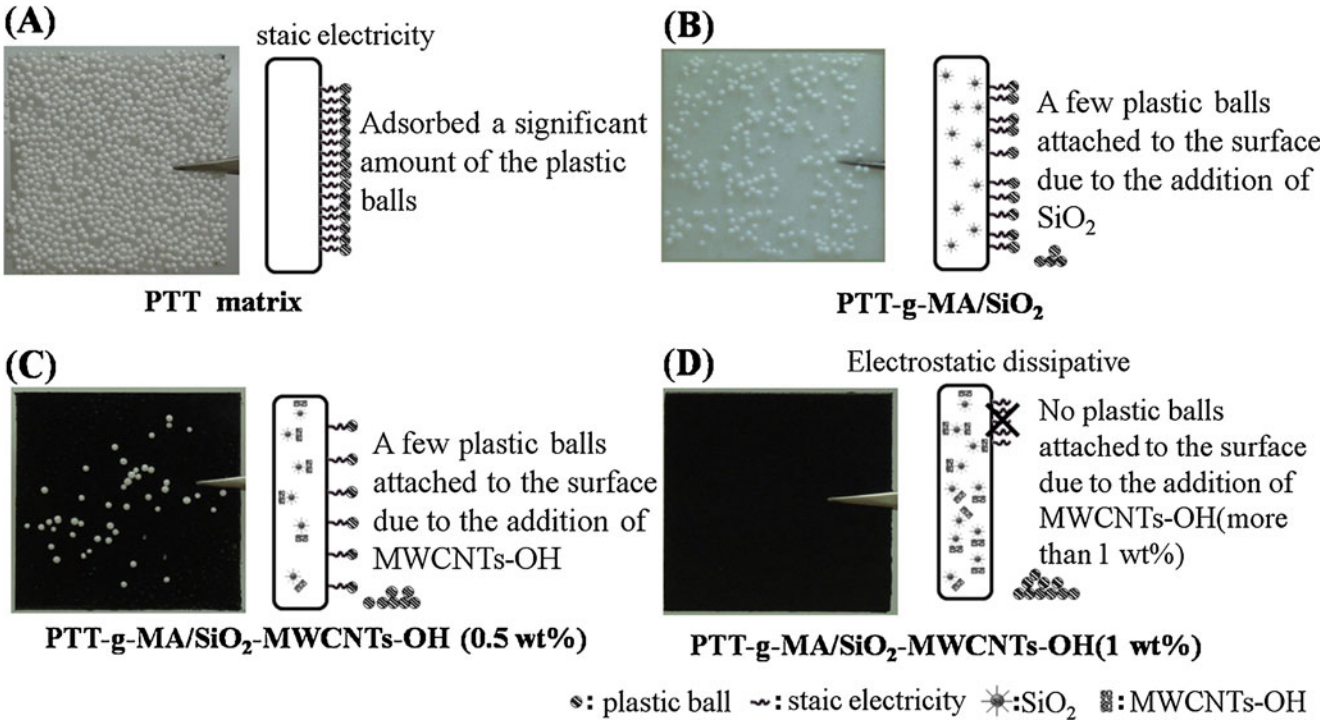

Fig. 9a–d Antistatic properties of **a** PTT, **b** PTT-*g*-MA/SiO_2-MWCNTs-OH (0.5 wt.%), **c** PTT-*g*-MA/SiO_2-MWCNTs-OH (1 wt.%), and **d** PTT-*g*-MA/SiO_2-MWCNTs-OH (2 wt.%) composites

are stronger than the hydrogen bonds formed in PTT/SiO_2-MWCNTs-OH, and are therefore more effective at hindering polymer motion. Moreover, the electrical resistivity of each PTT-*g*-MA/SiO_2-MWCNTs-OH hybrid was lower than that of its PTT/SiO_2-MWCNTs-OH equivalent, since the latter more easily forms the interconnected conductive pathway throughout the material [31]. The lower observed resistivities of the composites are consistent with an excess amount of SiO_2-MWCNTs-OH, which was physically dispersed throughout the polymer matrix. When the SiO_2-MWCNTs-OH loading is greater than 1 wt.%, the excess filler may have led to aggregate formation between the organic and inorganic phases, thereby reducing the compatibility of the matrix with PTT/SiO_2-MWCNTs-OH and PTT-*g*-MA/SiO_2-MWCNTs-OH.

Although the 1 wt.% PTT/SiO_2-MWCNTs-OH and PTT-*g*-MA/SiO_2-MWCNTs-OH composites exhibited resistivities as low as 3.5×10^7 and 1.1×10^6 Ω/sq, respectively, they cannot be classified as "conductive materials." They can, however, be considered "antistatic materials" [32]. The results of antistatic testing with pristine PTT-*g*-MA and PTT-*g*-MA/SiO_2-MWCNTs-OH (sample size: 4.50 cm diameter and 0.10 cm thick) are depicted in Fig. 9. Each film was rubbed and immersed in small plastic foam balls. Any adsorption of plastic balls would indicate the presence of static electricity. The pristine PTT-*g*-MA adsorbed a significant amount of plastic balls, whereas the 0.5 wt.% PTT-*g*-MA/SiO_2-MWCNTs-OH composite attracted only a few balls to its surface (Fig. 9b). Furthermore, both the 1 wt.% and 2 wt.% PTT-*g*-MA/SiO_2-MWCNTs-OH composites (Fig. 9c and d) had no adsorbed balls because of their lower electrical resistivities ($<10^7$ Ω/sq). Although the electrical resistivity of the 0.5 wt.% PTT-*g*-MA/SiO_2-MWCNTs-OH (9.8×10^8 Ω/sq) was in the range seen for "dissipative materials," there were still a few plastic balls adsorbed on the surface. The electrostatic dissipative property of the 0.5 wt.% sample was low compared with that of the 1 wt.% (1.1×10^6 Ω/sq) and 2 wt.% (1.2×10^4 Ω/sq) samples. This result indicated that samples exhibit absolute electrostatic dissipation when the electrical resistivity is $<10^7$ Ω/sq. Thus, the addition of SiO_2-MWCNTs-OH to the composite resulted in electrostatic dissipative properties in the bulk material, especially when the SiO_2-MWCNTs-OH content was more than 1 wt.%.

Conclusions

The synthesis of PTT-*g*-MA/SiO_2-MWCNTs-OH composites was accomplished using a simple melt-blending method. We demonstrated that SiO_2-MWCNTs-OH can be incorporated into PTT-*g*-MA copolymer through the formation of strong covalent bonds produced from the reaction between the MA groups of PTT-*g*-MA and hydroxyl groups of SiO_2-MWCNTs-OH. FTIR and ^{13}C solid-state NMR spectral analyses demonstrated that the MA was grafted onto the PTT copolymer and that ester bonds were formed in the PTT-*g*-MA/SiO_2-MWCNTs-OH hybrid. The newly formed ester

bonds may have been produced through the dehydration of MA groups in the PTT-*g*-MA matrix with grafted hydroxyl groups in the SiO_2-MWCNTs-OH. The PTT-*g*-MA/SiO_2-MWCNTs-OH was more readily suspended in phenol/tetrachloroethane solution because of the higher solubility of the polymer chains and the covalent linkages between the constituents. TEM images of the composites revealed the formation of SiO_2-MWCNTs-OH aggregates at high SiO_2-MWCNTs-OH loadings. DSC analysis indicated that the difference between the T_g and the T_m for the PTT-*g*-MA/SiO_2-MWCNTs-OH hybrid was smaller than that for the PTT/SiO_2-MWCNTs-OH hybrid. The PTT-*g*-MA/SiO_2-MWCNTs-OH (1 wt.%) composites exhibited significantly improved IDT, which was increased by 28 °C, and the residual yield improved by 32 %. This implied that the compatibility between PTT and SiO_2-MWCNTs-OH was enhanced. The electrical resistivity of the PTT-*g*-MA/MWCNTs-OH (1 wt.%) composite was 1.1×10^6 Ω/sq, which is 10^9-fold lower than that of neat PTT, which enhanced antistatic behavior. Thus, the current study demonstrates an enhancement in the compatibility between PTT and SiO_2-MWCNTs-OH, with consequent improvements in electrical conductivity and antistatic behavior.

Acknowledgments The author is grateful to the National Science Council (Taipei City, Taiwan, R.O.C.) for financial support (NSC 101-2622-E-244-001-CC3).

References

1. Lima LT, Aurasb R, Rubinob M (2008) Prog Polym Sci 33:820–852
2. Mohanty AK, Misraa M, Hinrichsen G (2000) Macromol Mater Eng 1:1–24
3. Gao Q, Zhu Q, Guo Y, Yang CQ (2009) Ind Eng Chem Res 48:9797–9803
4. Dalir H, Farahani RD, Nhim V, Samson B (2012) Langmuir 281: 791–803
5. Zheng L, Li C, Zhang D, Guan G, Xiao Y, Wang D (2011) Polym Int 60:666–675
6. Kwak G, Takagi A, Fujiki M (2005) Macromolecules 38:4169–4175
7. Liu W, Mohanty AK, Drzal LT, Misra M, Kurian JV, Miller RW (2005) Ind Eng Chem Res 44:857–862
8. Ronkvist AM, Xie W, Lu W, Richard AG (2009) Macromolecules 42:5128–5138
9. Chang JH, Kim SJ, Im S (2004) Polymer 45:5171–5181
10. Wu T, Li Y, Wu Q, Song L, Wu G (2005) Eur Polym J 41:2216–2223
11. Yamen M, Ozkaya S, Vasanthan N (2008) J Polym Sci Pol Phys 46: 1497–1504
12. Gupta A, Choudhary V (2012) J Appl Polym Sci 123:1548–1556
13. Ramontja J, Ray SS, Pillai SK, Luyt AS (2009) Macromol Mater Eng 294:839–846
14. Chang JH, Mun MK, Kim JC (2006) J Appl Polym Sci 102:4535–4545
15. Gupta A, Choudhary V (2011) Comp Sci Tech 71:1563–1568
16. Kim JY, Park HS, Kim SH (2007) J Appl Polym Sci 103:1450–1457
17. Yang Y, Gupta MC, Dudley KL, Lawrence RW (2005) Nano Let 5: 2131–2134
18. Thomassin JM, Lou X, Pagnoulle C, Saib A, Bednarz L, Huynen I (2007) J Phys Chem C 111:11186–11192
19. Mani R, Bhattarya M, Tang J (1999) J Polym Sci Pol Chem 37:1693–1702
20. Yao C, Yang G (2010) Polym Int 59:492–500
21. Wang D, Sun G (2011) J Appl Polym Sci 119:2302–2309
22. Pöllänen M, Pelz U, Suvanto M, Pakkanen TT (2010) J Appl Polym Sci 116:1218–1225
23. Xu J, Bartels JW, Bohnsack DA, Tseng TC, Mackay ME, Wooley KL (2008) Adv Funct Mater 18:2733–2744
24. Kameda T, Miyazawa M, Murase S (2005) Magn Reson Chem 43: 21–26
25. Wu CS (2005) J Polym Sci Pol Chem 43:1690–1701
26. Park KC, Mahiko T, Morimoto S, Takeuchi K, Endo M (2008) Appl Surf Sci 254:7438–7445
27. Cui W, Du F, Zhao J, Zhang W, Yang Y, Xie X (2011) Carbon 49: 495–500
28. Xu Y, Gao C, Kong H, Yan D, Jin YZ (2004) Macromolecules 37: 8846–8853
29. Ariffin H, Nishida H, Shirai Y, Hassan MA (2008) Polym Degrad Stab 93:1433–1439
30. Ahuja T, Kumar D, Singh N, Biradar AM (2001) Mater Sci Eng C 31: 90–94
31. Dudler V, Grob MC, Merian D (2000) Polym Degrad Stab 68:373–379
32. Narkis M, Lidor G, Vaxman A, Zuri L (1999) J Electrostat 47:201–214